Blind spatial unmixing of multispectral images: new methods combining sparse component analysis, clustering and non-negativity constraints

Moussa Sofiane Karoui [a,b,c,*], Yannick Deville [b], Shahram Hosseini [b], and Abdelaziz Ouamri [c]

[a] Division Observation de la Terre, Centre des Techniques Spatiales, 31200 Arzew, Algeria.

[b] Institut de Recherche en Astrophysique et Planétologie, Université de Toulouse, UPS-OMP, CNRS, 31400 Toulouse, France.

[c] Laboratoire Signaux et Images, Université des Sciences et de la Technologie d'Oran, 31000 Oran, Algeria.

E-mail addresses:

Sofiane.Karoui@irap.omp.eu (M.S. Karoui)

Yannick.Deville@irap.omp.eu (Y. Deville)

Shahram.Hosseini@irap.omp.eu (S. Hosseini)

ouamri@yahoo.com (A. Ouamri)

[*] Corresponding author. Address for correspondence: Centre des Techniques Spatiales, 01 Avenue de la Palestine, BP 13, 31200, Arzew, Algeria. Tel.: +213 41 47 22 17; fax +213 41 47 36 65

Abstract

Remote sensing has become an unavoidable tool for better managing our environment, generally by realizing maps of land cover using classification techniques. Traditional classification techniques assign only one class (e.g., water, soil, grass) to each pixel of remote sensing images. However, the area covered by one pixel contains more than one surface component and results in the mixture of these surface components. In such situations, classical classification is not acceptable for many major applications, such as environmental monitoring, agriculture, mineral exploration and mining, *etc*. Most methods proposed for treating this problem have been developed for hyperspectral images. On the contrary, there are very few automatic techniques suited to multispectral images. In this paper, we propose new unsupervised spatial methods (called 2D-Corr-NLS and 2D-Corr-NMF) in order to unmix each pixel of a multispectral image for better recognizing the surface components constituting the observed scene. These methods are related to the blind source separation (BSS) problem, and are based on sparse component analysis (SCA), clustering and non-negativity constraints. Our approach consists in first identifying the mixing matrix involved in this BSS problem, by using the first stage of a spatial correlation-based SCA method with very limited source sparsity constraints, combined with clustering. Non-negative least squares (NLS) or non-negative matrix factorization (NMF) methods are then used to extract spatial sources. An important advantage of our proposed methods is their applicability to the possibly globally underdetermined, but locally (over)determined BSS model in multispectral remote sensing images. Experiments based on realistic synthetic mixtures and real multispectral images collected by the Landsat ETM+ and the Formosat-2 sensors are performed to evaluate the performance of the proposed approach. We also

show that our methods significantly outperform the sequential maximum angle convex cone (SMACC) method.

Keywords

Multispectral spatial unmixing

Blind source separation

Sparse component analysis

Correlation

Clustering

Non-negativity constraints

1. Introduction

Thanks to the technological advances which occurred during the last decades in the signal and image processing fields, remote sensing has become an unavoidable tool for better understanding and managing our environment. Multispectral and hyperspectral imaging systems are the most powerful tools in the field of remote sensing. While hyperspectral sensors collect data in contiguous narrow bands (up to several hundred bands) in the electromagnetic spectrum, multispectral sensors provide images with a few relatively large bands. Both of these imaging systems are able to yield images in which single pixels have spectral content relevant to specifications of the observed scene and generally have common applications, such as environmental monitoring, agriculture, mineral exploration and mining, *etc*. Indeed, while hyperspectral imaging systems have a very high spectral discrimination capability, multispectral imaging systems are designed to support applications by providing bands that detect information in specific combinations of desired domains of the spectrum.

Analysis methodologies for remote sensing (multi/hyperspectral) images generally lead to maps of land cover by using classification techniques. Traditional classification algorithms assign one and only one class (e.g., water, soil, grass) of land to each pixel. However, the spectral vector associated with each pixel may be a mixture of contributions from pure materials (pure elements or endmembers) contained in the observed area [23]. Alternatively, each band of a remote sensing image corresponding to a given spectral channel may be considered as a specific mixture of the images respectively associated with each endmember [21,22]. In such situations, traditional classification techniques are not acceptable for many major applications. Blind source separation (BSS) methods are attractive in this framework, because they aim at restoring

unknown source "signals", only based on the knowledge of the observed mixtures of these signals [7]. Applying such BSS methods to a remote sensing image, one can therefore hope to extract each endmember image, which then leads to better recognition of the surface components constituting the observed scene.

Significant efforts are made by the scientific community in the considered framework. Most BSS methods have been developed for *hyperspectral* images, since these images allow one to take advantage of the large number of available spectral bands. These BSS methods are based on the following three main concepts: geometrical, statistical and sparse regression concepts (see e.g. the reviews of classical methods in [3,35]). Many of these methods are not applicable to *multispectral* images, because of the limited number of spectral bands of these images. Designing BSS methods for extracting endmember images from multispectral data therefore represents an important challenge. Indeed, there exist many situations in which hyperspectral images may not always be available in addition to multispectral images for a given area imposed by the considered application. Very few automatic BSS methods [12,25] suited to multispectral images are available in the literature. Therefore, we here propose new hybrid unsupervised BSS methods intended for multispectral images.

In remote sensing images, the mixture is most often assumed to be linear and instantaneous [3,12,13,17,23,31,33,35-38]. A mixture is stated to be "linear and *instantaneous*" if each observation is a weighted sum of *unshifted* versions of the source signals, where the considered shift is related to the variable(s) on which the considered signals depend. These weights then form the so-called mixing matrix. When considering a multispectral image as combinations of source images measured in various spectral bands (respectively as combinations of spectra measured at various locations), the

mixture is instantaneous if the value measured at any location (resp. in any given spectral band) only depends on the source images at the same location (resp. on the source spectra in the same band). Thus, we assume that the reflectance spectrum of a pixel is the result of linear instantaneous combination of the endmember spectra within the pixel and the weight of each endmember spectrum is the percentage (or abundance fraction) of that endmember in the area covered by the pixel.

Most BSS techniques developed since the first papers by Herault et al. [15,16,20] concern linear instantaneous mixtures and are based on independent component analysis (ICA) (see e.g. the review of classical methods in [7]). ICA consists in representing the initial observations as linear mixtures of statistically independent components, and therefore assumes the sources to be statistically independent. More recently, other methods have been proposed for solving the BSS problem. This especially includes methods based on sparse component analysis (SCA) [1,7,8,19], which exploit the sparsity properties of sources in different representation domains. Most approaches based on ICA (resp. SCA) provide a unique theoretical solution, equal to the sources (up to permutation and scale indeterminacies), for the BSS problem under the source independence constraint (resp. source sparsity constraint). In practice, this solution is reached up to estimation errors. The estimated sources thus obtained in environment sciences may not fulfill the non-negativity condition of the original data, which limits the attractiveness of ICA and SCA methods in this application field (note also that the independence constraint on sources is not guaranteed for these data [32]).

When the sources and mixing coefficients are non-negative, as in remote sensing images, a third class of BSS approaches may be used, i.e. non-negative matrix factorization (NMF) [5,6], which consists in representing the initial non-negative

observations as non-negative linear mixtures of non-negative components [28,29]. However, standard NMF methods have limitations, i.e. they do not provide a unique solution [9] and their convergence point depends on their initialization.

Non-negativity constraints are also used in the non-negative least squares (NLS) method, which may be considered for representing the initial observations as linear mixtures of non-negative components [27]. However, NLS alone cannot be used to perform *blind* source separation, i.e. to estimate both the sources and mixing matrix: unlike NMF, NLS is a *non-blind* method, since it determines the coefficients involved in the decomposition of an observed vector on a set of *known* vectors. In the considered conditions, NLS has the advantage of providing a unique solution.

Our proposed methods, called 2D-Corr-NLS and 2D-Corr-NMF, avoid the limitations which are specific to each of the above-mentioned approaches. Our methods combine the first stage of a spatial correlation-based SCA algorithm (which consists in detecting single-source zones, defined hereafter) with very mild assumptions about source sparsity, and clustering to derive a non-negative estimate of the mixing matrix (corresponding to the endmember spectra). This matrix is then used as an input of NLS or NMF methods, in order to unmix each pixel of a multispectral image and to extract non-negative spatial sources (abundance maps). An important advantage of our approach is its applicability to possibly globally underdetermined, but locally (over)determined mixing models, as detailed further in this paper.

This paper is organized as follows. In Section 2, we provide a general definition of the BSS problem, and we derive two approaches for applying BSS methods to remote sensing multispectral images, based on alternative data models. In Section 3, we describe our overall methodology, and we explain our approach to evaluate test results.

Section 4 consists of experimental results. In that section, we describe the used data and studied areas, and we compare our results with those obtained with the sequential maximum angle convex cone (SMACC) method [12]. Finally, we end up by a conclusion in Section 5.

2. Standard data model of BSS and application to remote sensing

2.1. Standard data model of BSS

Generally speaking, BSS methods aim at restoring a set of L unknown source signals s_j from a set of K observed signals x_i which are mixtures of these source signals [7]. This separation is said to be "blind" when the sources and the parameters of the mixture are assumed to be unknown. The source-observation relationship reads

$$x = \mathcal{F}(s), \tag{1}$$

where $s = [s_1 \dots s_L]^T$ and $x = [x_1 \dots x_K]^T$ are the source and observation vectors corresponding to a single measurement, and $\mathcal{F}(.)$ denotes the mixing operator. In the simplest BSS configuration, one considers linear instantaneous mixtures of the sources in the determined case, i.e., $L=K$. Then, $\mathcal{F}(.)$ reduces to a square, constant, and supposedly invertible mixing matrix A (containing mixing coefficients) and the observations read

$$x = A\, s. \tag{2}$$

BSS would then ideally consist in deriving an estimate $\hat{A}$ of A, so as to then determine the output vector

$$y = \hat{A}^{-1}\, x = \hat{A}^{-1}\, A\, s. \tag{3}$$

Each component y_j of this vector y would then be equal to the source signal having the same index, i.e. to s_j. It is well-known however that, without additional assumptions,

this can only be achieved up to two types of indeterminacies, which respectively concern the order (permutation indeterminacy) and scale factors with which the source signals appear in the output vector *y*.

In this paper, we aim at taking advantage of the BSS techniques in the field of remote sensing. Starting from the linear instantaneous mixing assumption in multispectral remote sensing images, according to the BSS terminology, the question is: how can these observations be expressed in terms of the mixing matrix and the sources which are involved in the standard BSS data model (2)? This yields two alternative answers, based on different approaches, as explained below.

2.2. Intuitive approach of remote sensing: spectral sources

As explained in Section 1, we may consider each spectral row vector associated with a pixel in a multispectral image as a linear instantaneous mixture of the spectra associated with *L* pure materials (the *K* pixels are here seen as a one-dimensional array). The entries of each such row vector correspond to the *N* spectral bands. By gathering all these data samples, we obtain a data model which is coherent with (2) and which reads

$$\begin{pmatrix} x_1(1) & \dots & x_1(N) \\ \vdots & \ddots & \vdots \\ x_K(1) & \dots & x_K(N) \end{pmatrix} = \begin{pmatrix} a_{11} & \dots & a_{1L} \\ \vdots & \ddots & \vdots \\ a_{K1} & \dots & a_{KL} \end{pmatrix} \cdot \begin{pmatrix} s_1(1) & \dots & s_1(N) \\ \vdots & \ddots & \vdots \\ s_L(1) & \dots & s_L(N) \end{pmatrix}, \quad (4)$$

where $x_i(n)$ is the n^{th} spectral component of the i^{th} pixel, $s_j(n)$ is the n^{th} spectral component of the j^{th} pure material and a_{ij} is the abundance fraction of the j^{th} pure material in the i^{th} pixel. Then, we call "(spectral) sources" the pure material spectra, and each observation corresponds to one pixel of the multispectral image. The two-dimensional array representation of this approach is given in Fig. 1(a). In addition, these data meet the following natural constraints

$$s_j(n) \geq 0,\ a_{ij} \geq 0 \text{ and } \sum_j a_{ij} = 1,\ \forall \begin{array}{l} i = 1...K \\ j = 1...L \\ n = 1...N \end{array}. \quad (5)$$

Applying BSS methods requires "many" samples, which here means "many" spectral bands. This approach therefore only applies to hyperspectral images, whereas we consider multispectral images with a low number N of bands in this paper. To solve this issue, we introduce another approach hereafter.

2.3. Alternative approach for remote sensing: spatial sources

An interesting alternative consists in transposing (4). Hence, we get

$$\begin{pmatrix} x_1(1) & \dots & x_K(1) \\ \vdots & \ddots & \vdots \\ x_1(N) & \dots & x_K(N) \end{pmatrix} = \begin{pmatrix} s_1(1) & \dots & s_L(1) \\ \vdots & \ddots & \vdots \\ s_1(N) & \dots & s_L(N) \end{pmatrix} \cdot \begin{pmatrix} a_{11} & \dots & a_{K1} \\ \vdots & \ddots & \vdots \\ a_{1L} & \dots & a_{KL} \end{pmatrix}. \quad (6)$$

To simplify the presentation with respect to the BSS terminology, we rewrite (6) with the following notations

$$\begin{pmatrix} \bar{x}_1(1) & \dots & \bar{x}_1(K) \\ \vdots & \ddots & \vdots \\ \bar{x}_N(1) & \dots & \bar{x}_N(K) \end{pmatrix} = \begin{pmatrix} \bar{a}_{11} & \dots & \bar{a}_{1L} \\ \vdots & \ddots & \vdots \\ \bar{a}_{N1} & \dots & \bar{a}_{NL} \end{pmatrix} \cdot \begin{pmatrix} \bar{s}_1(1) & \dots & \bar{s}_1(K) \\ \vdots & \ddots & \vdots \\ \bar{s}_L(1) & \dots & \bar{s}_L(K) \end{pmatrix}. \quad (7)$$

Now, $\bar{x}_n(i)$ represents the n^{th} spectral component of the i^{th} pixel, $\bar{a}_{nj}$ is the n^{th} spectral component of the j^{th} pure material and $\bar{s}_j(i)$ represents the abundance fraction of the j^{th} pure material in the i^{th} pixel. Consequently, each "(spatial) source" here corresponds to all abundance fractions of one pure material in all pixels, and each observation corresponds to one spectral band of the multispectral image. The two-dimensional array representation of this approach is given in Fig. 1(b). The above request for "many" samples in BSS methods here means "many" pixels, so that this constraint is usually met. This approach thus also applies to multispectral images with few spectral bands and is therefore less restrictive than the previous one from that point of view. This is

therefore the only method considered in the rest of this paper. For the sake of readability, the "bars" are therefore removed from the notations used for the sources, mixing coefficients and observations in the next sections (i.e. $s_j(i)$ instead of $\bar{s}_j(i)$ and so on), but it should be clear that these notations refer to the mixing model (7), not the model (4). Besides, the above-defined natural constraints (5) here read

$$\bar{a}_{nj} \geq 0,\ \bar{s}_j(i) \geq 0 \text{ and } \sum_j \bar{s}_j(i) = 1,\ \forall \begin{array}{l} i = 1...K \\ j = 1...L \\ n = 1...N \end{array}. \quad (8)$$

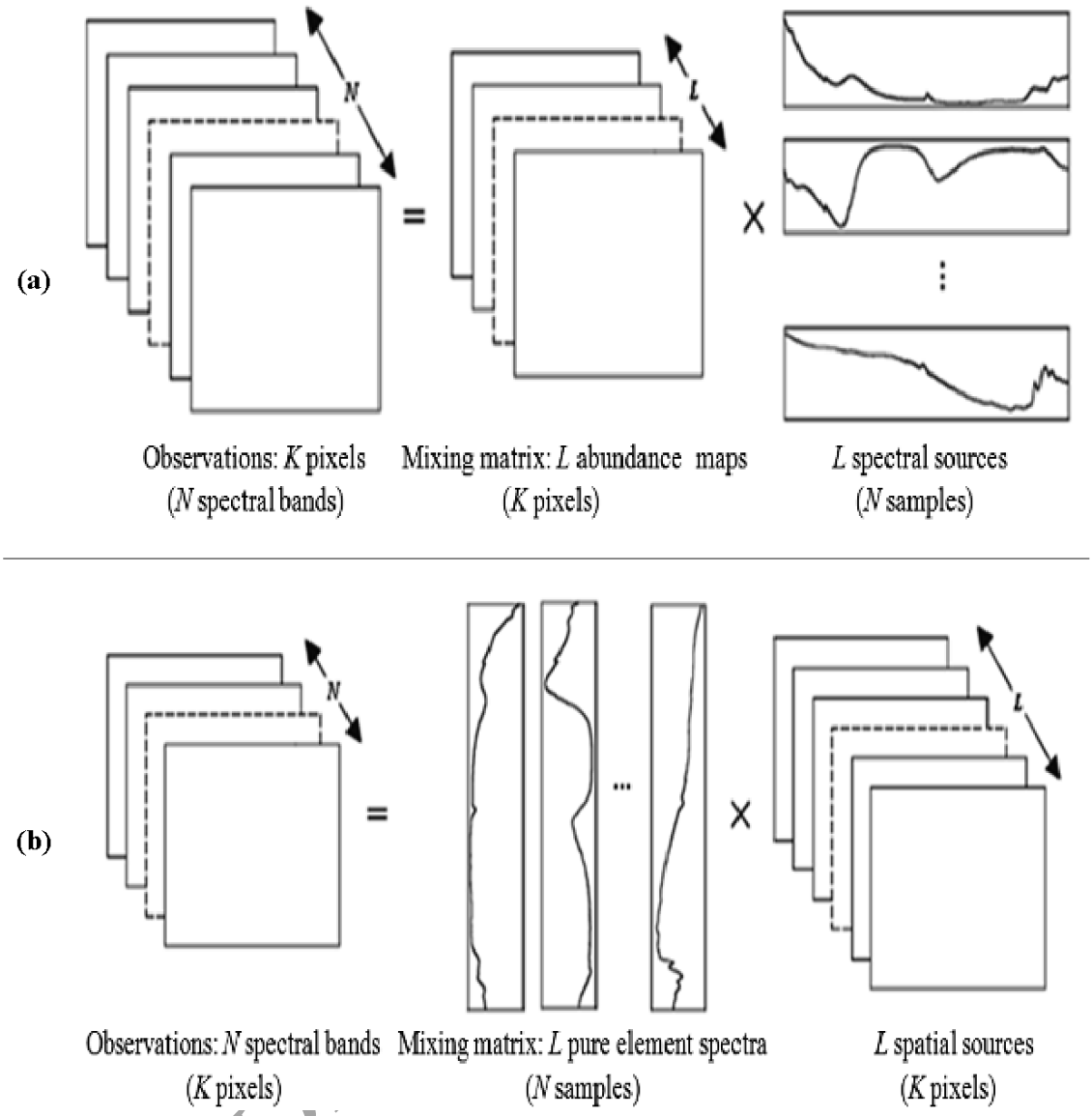

Figure 1. Data model based on (a) spectral sources, (b) spatial sources.

3. Proposed unmixing methods

The first stage of the unmixing methods proposed in this paper is based on SCA. Some SCA methods require the sources to have no overlap in the considered representation domain [7,19], which is quite restrictive. On the contrary, only a few zones should contain no overlapping sources in the spatial domain when using the first stage (which is based on the SCA approaches that we proposed in [8,30]) of the methods that we introduce below. The spatial domain is divided into small zones denoted as Ω, and that

we call "analysis zones". These 2-dimensional zones consist of adjacent pixels: the pixel values corresponding to band p are denoted as $x_p(i)$ hereafter, i.e. using a single pixel index i for the sake of readability, but we do take into account the 2-dimensional structure of the images in our approach. The spatial domain is explored using adjacent or overlapping analysis zones. In each zone Ω, we consider the cross-correlation coefficients $\rho_{x_p x_q}(\Omega)$ between the non-centered observed signals $x_p(i)$ and $x_q(i)$. To this end, all the pixel values $x_p(i)$ of signal x_p (resp. x_q) over the analysis zone Ω are rearranged as a one-dimensional vector denoted $x_p(\Omega)$ (resp. $x_q(\Omega)$). The cross-correlation coefficient of these signals over this analysis zone is then defined as

$$\rho_{x_p x_q}(\Omega) = \frac{< x_p(\Omega), x_q(\Omega) >}{\left\| x_p(\Omega) \right\| . \left\| x_q(\Omega) \right\|}, \ \forall \ p, q = 1 \ldots N \text{ and } p > q, \tag{9}$$

where the notations <., .> and ||.|| respectively stand for the inner product and vector norm.

The methods introduced hereafter are based on some assumptions and definitions. These assumptions and definitions, which concern the abundance fractions of pure materials in the spatial domain, are gradually introduced when describing the different stages of the proposed methods.

3.1. Unmixing methods

The proposed methods operate in different stages described hereafter.

3.1.1. The detection stage

This stage consists in automatically detecting the analysis zones in which pure materials are isolated (assuming all pure materials are accessible). These zones are called single-source zones (i.e. they consist of pure pixels with the same pure material). An isolated and accessible pure material is defined as follows:

Definition 1 *A pure material is said to be "isolated" in an analysis zone if only this pure material is present in this zone, i.e., yields a non-zero vector $s_j(\Omega)$ with elements $s_j(i)$ in this zone.* The abundance fraction of this pure material is then equal to one for any pixel in this zone, due to (8).

Definition 2 *A pure material is said to be "accessible" in the spatial domain if there exist at least one analysis zone where it is isolated.*

The existence of at least one single-source zone for each pure material in a multispectral image is expressed by the following assumption:

Assumption 1 *Each pure material is accessible in the spatial domain.*

The above sparsity assumption in the spatial domain is quite realistic for high spatial resolution multispectral images, because they contain spatial zones which each correspond to a single pure material and which have a large enough extent (in pixels) at this resolution.

Detection of the single-source zones is performed using the following property:

Property 1 *A necessary and sufficient condition for a pure material to be isolated in a zone* Ω *is*

$$|\rho_{xpxq}(\Omega)| = 1, \ \forall \ p, q = 1 \ldots N \text{ and } p > q. \tag{10}$$

To demonstrate this property, we introduce the following assumptions:

Assumption 2 *Over each analysis zone, the non-zero vectors $s_j(\Omega)$ are linearly independent (if there exist at least two such vectors in this zone).*

The above assumption sets a constraint on the sources (abundance fractions), but this constraint is much less stringent than those (such as source statistical independence) which are set by many BSS methods. Moreover, Assumption 2 is especially expected to be met in the application considered in this paper, because the abundance fractions sum

to one in each pixel, and therefore the source vectors $s_j(\Omega)$ for a given analysis zone Ω containing M pixels sum to the M-dimensional vector 1_M, whose entries are all equal to 1. More precisely, consider the case when only two source vectors $s_j(\Omega)$ and $s_{j'}(\Omega)$ are non-zero over a zone Ω. Then, as shown by (8), we have $s_j(\Omega) + s_{j'}(\Omega) = 1_M$. If $s_j(\Omega)$ and $s_{j'}(\Omega)$ are linearly dependent, they also meet the condition $c_1 s_j(\Omega) + c_2 s_{j'}(\Omega) = 0_M$, where c_1 and c_2 are two constants not both equal to 0. By solving the above two equations, it may easily be shown that this case corresponds to the situation when s_j and $s_{j'}$ are constant over all the considered zone Ω. This case is therefore very specific, so that excluding it in Assumption 2 is not restrictive: it is not a surprise that a BSS method cannot separate two sources if both remain constant.

Assumption 3 *In any analysis zone, the sub-matrix composed of the columns of A corresponding to pure materials present in this zone has full column rank.*

Proof of property 1 For each analysis zone, (2) yields

$$x_p(\Omega) = \sum_{j=1}^{L} a_{pj} s_j(\Omega), \ \forall \ p = 1 \ldots N. \tag{11}$$

Besides, applying the Cauchy-Schwarz inequality to (9) shows that

$$|\rho_{x_p x_q}(\Omega)| \leq 1, \ \forall \ p, q = 1 \ldots N \text{ and } p > q, \tag{12}$$

with equality if and only if $x_p(\Omega)$ and $x_q(\Omega)$ are linearly dependent.

If only one pure material, with index j, is present in a considered analysis zone Ω, and assuming that all mixing coefficients a_{pj} are non-zero, (11) shows that all observations $x_p(\Omega)$, with $p = 1 \ldots N$, are collinear. Therefore, equality holds whatever p and q in (12) and the detection condition (10) is fulfilled.

Now, we suppose that at least two pure material vectors $s_j(\Omega)$ are non-zero. It may easily be shown that, if $x_p(\Omega)$ and $x_q(\Omega)$ were linearly dependent for all p and q, with $p, q = 1 \ldots N$ and $p > q$, then, due to Assumption 2, all the columns of the mixing

matrix A, with indices equal to the indices of non-zero pure material vectors, would be collinear. This is not true due to Assumption 3. Therefore, in this case, at least one pair of vectors ($x_p(\Omega)$, $x_q(\Omega)$) does not consist of linearly dependent vectors, so that condition (10) is not fulfilled. This completes the proof of Property 1.

Let us stress that we here consider the non-centered version of the observations because, in our application where abundance fractions sum to one, applying the counterpart of Property 1 to the centered version of the signals (which is used in other applications [8,30]) would not allow us to perform single-source zone detection. Indeed, if two pure material vectors $s_j(\Omega)$ and $s_{j'}(\Omega)$ are non-zero, the abundance fraction sum-to-one constraint yields

$$s_j(\Omega) + s_{j'}(\Omega) = 1_M. \tag{13}$$

For the centered versions $S_j(\Omega)$ and $S_{j'}(\Omega)$ of the sources, (13) becomes

$$S_j(\Omega) + S_{j'}(\Omega) = 0_M. \tag{14}$$

For all p and q, with $p, q = 1 \ldots N$ and $p > q$, (2) yields for the centered versions $X_p(\Omega)$ and $X_q(\Omega)$ of the observations

$$\begin{cases} X_p(\Omega) = a_{pj} S_j(\Omega) + a_{pj'} S_{j'}(\Omega) \\ X_q(\Omega) = a_{qj} S_j(\Omega) + a_{qj'} S_{j'}(\Omega) \end{cases}. \tag{15}$$

Due to (14), Eq. (15) becomes

$$\begin{cases} X_p(\Omega) = (a_{pj} - a_{pj'}) S_j(\Omega) \\ X_q(\Omega) = (a_{qj} - a_{qj'}) S_j(\Omega) \end{cases}. \tag{16}$$

In this case, $X_p(\Omega)$ and $X_q(\Omega)$ are collinear. Then, the centered detection condition (i.e. the centered version of (10)) is fulfilled, despite the presence of two (possibly linearly independent) pure materials in the considered analysis zone.

Property 1 is used as follows in our BSS methods. For each analysis zone, we compute the following parameter

$$\min_{p,q} (|\rho_{Xp Xq}(\Omega)|), \ \forall\, p, q = 1 \ldots N \text{ and } p > q. \tag{17}$$

The mean or maximum of these correlation coefficients may be used instead, but their minimum sets the most restrictive constraint. If this parameter (17) exceeds a threshold value (close to 1 and set to 0.992 in our investigations, based on test results), we consider that this analysis zone is a single-source zone.

3.1.2. The estimation stage

This stage consists in computing estimates of all tentative columns of mixing matrix A. Every single-source zone Ω yields an estimate $\hat{a}_{.j}$ of one tentative column of the matrix (corresponding to one tentative endmember spectrum), using the following formula

$$\hat{a}_{.j} = \begin{pmatrix} median\,(x_1(\Omega)) \\ . \\ . \\ . \\ median\,(x_N(\Omega)) \end{pmatrix}. \tag{18}$$

Our motivation for using this approach may be defined as follows. In our application, all abundance fractions are positive and sum to one in each pixel. In a perfect single-source analysis zone, one abundance fraction is equal to one, while all other are zero. Each observation is then equal to the value of the mixing coefficient associated with that observation and with the present pure material, in each pixel of that zone. In practice, for each observation (i.e. for each band), using the median of all pixel values over the considered analysis zone yields an accurate estimate of the corresponding mixing coefficient. The method used in this estimation stage is therefore specific to the abundance fraction positiveness and sum-to-one constraints faced in the application considered in this paper, and different from the approach that we used in our above-mentioned previous SCA methods [8,30]. Note that the estimated columns thus obtained

are always non-negative, since they consist of medians of observed and therefore non-negative data.

If there are multiple single-source zones in a multispectral image where the same pure material is present, several estimates of the same endmember spectrum are obtained. Clustering is then an attractive approach to find a *single* estimated endmember spectrum (one column of estimated mixing matrix $\hat{A}$) for each pure material, and is used hereafter. In this subsequent stage, we associate the detection parameter (17) with each estimated column. Indeed, this parameter can be used as a confidence degree in the clustering stage, as detailed hereafter.

3.1.3. The clustering stage

This stage consists in selecting the L columns of estimated mixing matrix $\hat{A}$ from all the tentative columns estimated in the previous stage. Clustering or cluster analysis is an unsupervised learning tool for classifying heterogeneous data sets into homogeneous and separate groups (called clusters) with respect to a distance or similarity measure. Common distance measures are Euclidian distance, Manhattan distance, Mahalanobis distance and Hamming distance. The most popular approach to clustering is partitioning clustering [11].

The mostly used algorithms in partitioning clustering are k-means and its variants (fuzzy c-means, k-medians). These algorithms choose k initial centers, where k is a user-specified parameter corresponding to the number of desired clusters (i.e., the number of columns of $\hat{A}$ and of associated pure materials in our application). Each point (estimated column vector of mixing matrix in our application) of the data set is then assigned to the cluster with the closest center (column vector). The center of each cluster is then updated based on the average (for k-means and fuzzy c-means algorithms), or on the

median (for *k*-medians algorithm) of the points assigned to the cluster. These assignment and update steps are repeated until the assignments no longer change, or equivalently, until the centers remain the same.

In this paper, we use the fuzzy *c*-means algorithm. This algorithm sets the center of each cluster to the element with the highest degree of confidence. In this paper, we define the degree of confidence of any estimated column as the value of its detection parameter (17). The *L* columns are thus obtained in any order, which corresponds to the permutation indeterminacy of BSS methods. This indeterminacy is not an issue in our application. Note that the estimated matrix thus derived from all above-defined non-negative columns is also non-negative.

The fuzzy *c*-means algorithm requires setting different parameters. The most sensitive parameter is the number of clusters. Different choices of the number of clusters lead to different clustering results. Therefore, the estimation of the optimal number k^* of clusters is a prime concern. Many cluster validity indices have been proposed in order to estimate the optimal number of clusters [2,4,10,26,34,39]. Their computation is based on the following general procedure:

i) Apply the considered clustering algorithm for different values of *k*.

ii) Calculate the cluster validity index for each result.

iii) Choose the optimal number of clusters k^*.

In this paper, we use the cluster validity index described in [24].

3.1.4. The extraction stage

This stage consists in extracting the *L* non-negative spatial sources (abundance maps) under non-negativity constraints. Two alternative methods are used to this end in this

investigation. The first method is non-negative least squares (NLS). The NLS method introduced by Lawson and Hanson [27] solves the following matrix problem:

$$\textit{Minimize} \parallel \hat{A}\,\hat{s} - x \parallel \text{ subject to } \hat{s} \geq 0, \tag{19}$$

where the minimization is performed with respect to $\hat{s}$. In our approach, the NLS method is applied separately to each pixel position, so as to unmix the part of the multispectral image corresponding to that position. Thus, in (19), $\hat{A}$ represents the mixing matrix identified in the previous stage, x represents the spectral vector associated with the considered observed pixel, and $\hat{s}$ is the estimated vector of pure material abundance fraction values for that pixel. It should be noted that the NLS method sets no constraints on the signs of the elements of $\hat{A}$ and x, but requires the number of non-zero components of the estimated vector $\hat{s}$ to be at most equal to the number of components of the vector x (and NLS then provides a unique solution). The latter condition on $\hat{s}$ is met here, thanks to the following assumption:

Assumption 4 *The BSS model is locally (over)determined, i.e.,* $N \geq L(\Omega)$ *in any analysis zone* Ω, *where* $L(\Omega)$ *is the number of pure materials present in zone* Ω.

Let us stress here that in multispectral image configurations, the BSS model is generally globally underdetermined ($N < L$).

The second method used hereafter is non-negative matrix factorization (NMF). NMF, proposed by Lee and Seung [28,29], is a general matrix decomposition method. Given a non-negative N x K matrix X, NMF aims at finding a non-negative N x L matrix $\hat{A}$ and a non-negative L x K matrix $\hat{S}$, such that

$$X \approx \hat{A}\,\hat{S}. \tag{20}$$

As stated in Section 1, NMF methods are very sensitive to initialization: they do not always provide a unique solution. Indeed, any couple of non-negative matrices $(\hat{A}, \hat{S})$

which meets approximation (20) is a solution to NMF.

Unlike the NLS method, Lee and Seung's NMF alternating multiplicative update rules [29] are used in our approach to unmix a multispectral image as a whole and not pixel by pixel. The $\hat{A}$ matrix is here initialized with the non-negative mixing matrix identified in the clustering stage of our overall BSS method. The initial matrix $\hat{S}$ is derived from the observations and previously estimated mixing matrix, by means of NLS. Let us stress here, that the NMF method allows the updating of the estimated mixing matrix, which is attractive if it was not accurately identified in the previous stage.

Another important issue is the abundance fraction sum-to-one constraint. This natural constraint formulated in (8), can be handled by the NLS and NMF methods using a simple but effective technique as in [14]: we increase the observation and mixing matrices by a row containing a constant strictly positive value. The NLS matrix problem and the NMF alternating multiplicative update rules take these two extended matrices as inputs. Note also that the scale indeterminacy is here avoided thanks to this abundance fraction sum-to-one constraint.

The above-defined different stages constitute our two new proposed methods, respectively called **"2D-Corr-NLS"** and **"2D-Corr-NMF"**, for multispectral image spatial unmixing. The block diagram of the proposed methods is given in Fig. 2. In our tests, the 2D-Corr-NMF method yielded almost the same performance as the 2D-Corr-NLS method, and therefore the results of the 2D-Corr-NMF method will not be detailed in the next section.

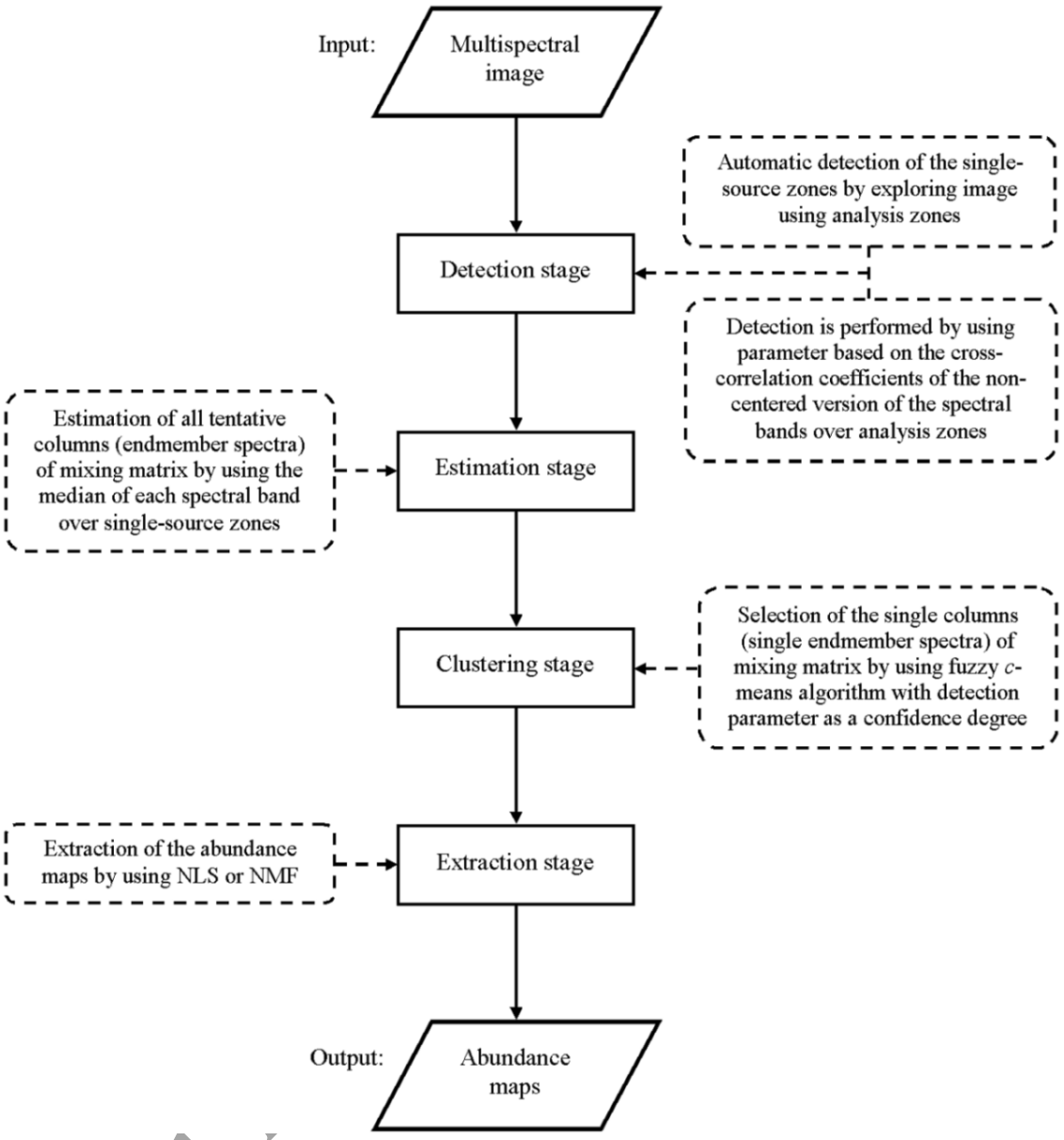

Figure 2. Block diagram of the proposed methods.

3.2. Performance evaluation criteria

For synthetic data, the normalized mean square error (NMSE) between the original and estimated abundance maps is used to evaluate the performance of the used methods. This criterion is defined as follows

$$NMSE_j = \frac{\left\| s_j - y_j \right\|^2_{Frobenius}}{\left\| s_j \right\|^2_{Frobenius}}, \ \forall \ j = 1 \ldots L, \tag{21}$$

where y_j is the estimate of s_j.

For real and synthetic data, another performance criterion is also designed. It consists in selecting one single-source zone, successively for each pure material composing the observations, where this pure material corresponds to a known endmember thanks to ground truth. Then, for each such zone, we separately consider each estimated abundance map, and we compute the mean value of this map over this zone. We thus build a validation matrix, whose entry with indices (*m, n*) is equal to the above-defined mean abundance for the analysis zone no. *m* (which actually contains pure material no. *m*) and for the estimated abundance map no. *n*. Each diagonal entry (*m, m*) of this validation matrix thus represents the extraction accuracy of abundance map no. *m* from the estimated abundance map of pure material no. *m*. It is close to one when our proposed methods succeed in correctly estimating the abundance maps. Similarly, the off-diagonal entries of the validation matrix represent the identification error. They are close to zero when our proposed methods succeed. Therefore, the mean of the diagonal entries represents the accuracy of the overall extraction of the abundance maps.

4. Experimental results

Experiments based on realistic synthetic mixtures of images and then on real multispectral images were performed to evaluate the performance of the proposed methods and of a method from the literature.

4.1. Synthetic data

Two datasets of synthetic but realistic sources (400x400-pixel abundance maps) are created from a real classification of land cover (by averaging pixel classification values on a sliding 5x5 window). The first dataset (Fig. 3(a)) contains eight sources (abundance maps). Each of them contains at least 1.5% of pure pixels. For each source, a four-value spectrum is randomly generated. Hence, a mixing matrix with eight columns and four rows is created. Then, taking into account all above-mentioned assumptions, four observations are generated by linearly mixing the sources. The four generated observations contain 56% of pure pixels. The second dataset (Fig. 3(b)) contains ten sources. Each of them contains at least 0.25% of pure pixels. Again, for each source, a four-value spectrum is randomly generated, and a mixing matrix with ten columns and four rows is created. This mixing matrix is used to linearly generate four observations from the sources (taking into account all above-mentioned assumptions). These observations contain 42% of pure pixels. Note here, that in the two datasets the mixture is globally underdetermined but pre-processed so as to be (over)determined on each analysis zone, by zeroing the lowest source values if required, and rescaling the remaining sources so that they sum to one.

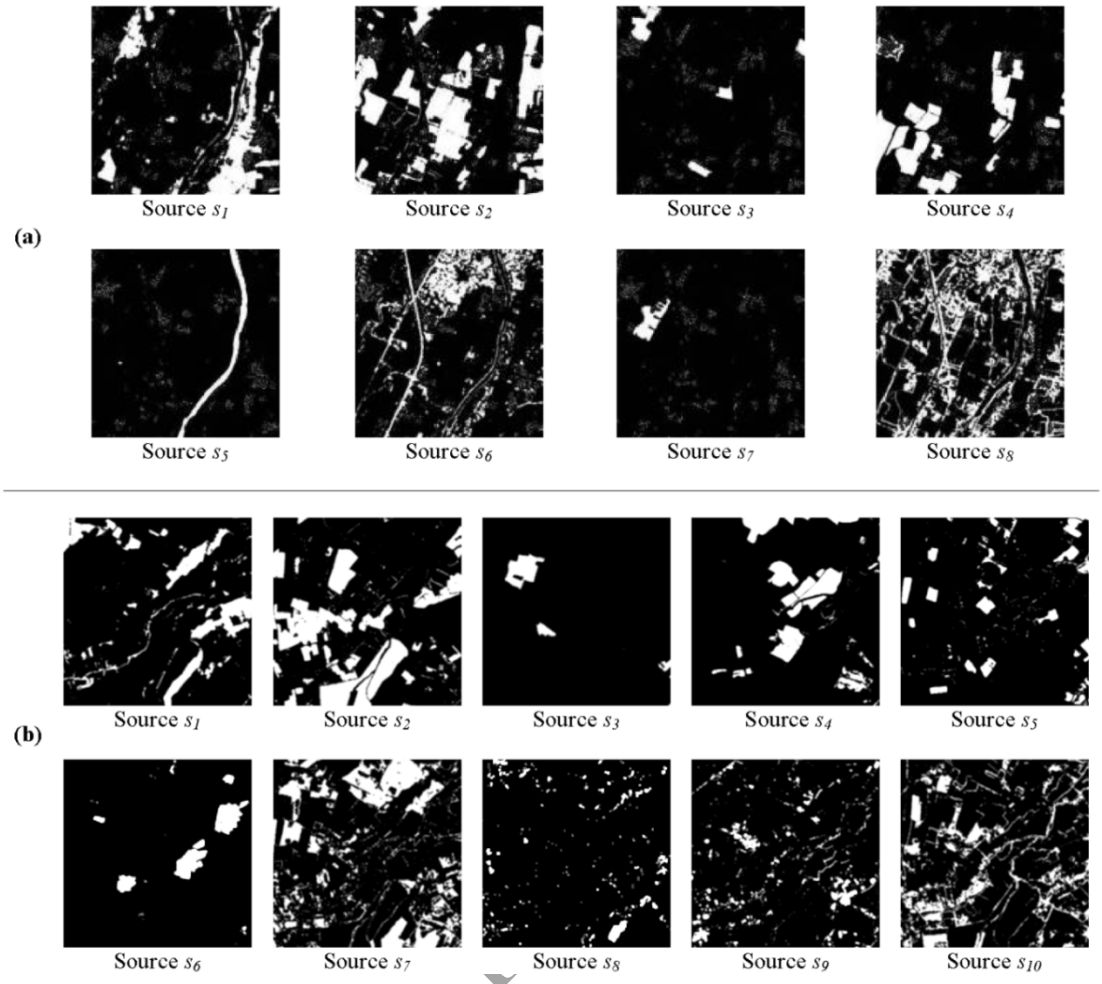

Figure 3. Original synthetic sources (abundance maps). (a) First dataset. (b) Second dataset.

4.2. Real data

Real multispectral images collected by the Landsat ETM+ and Formosat-2 sensors are also used. The Landsat ETM+ image with six spectral bands (Fig. 4(a)), and 30-meter spatial resolution, covers a part of Oran area (Algeria). This area is characterized by a difficult landscape and diversity of themes (urban area, forest, cereal cultivation, water, *etc*). The Formosat-2 image with four spectral bands (Fig. 4(b)), and 8-meter spatial resolution, covers a part of Toulouse area (France). This area is also characterized by a diversity of themes. The studied areas offer us a great interest for testing and evaluating the proposed methods.

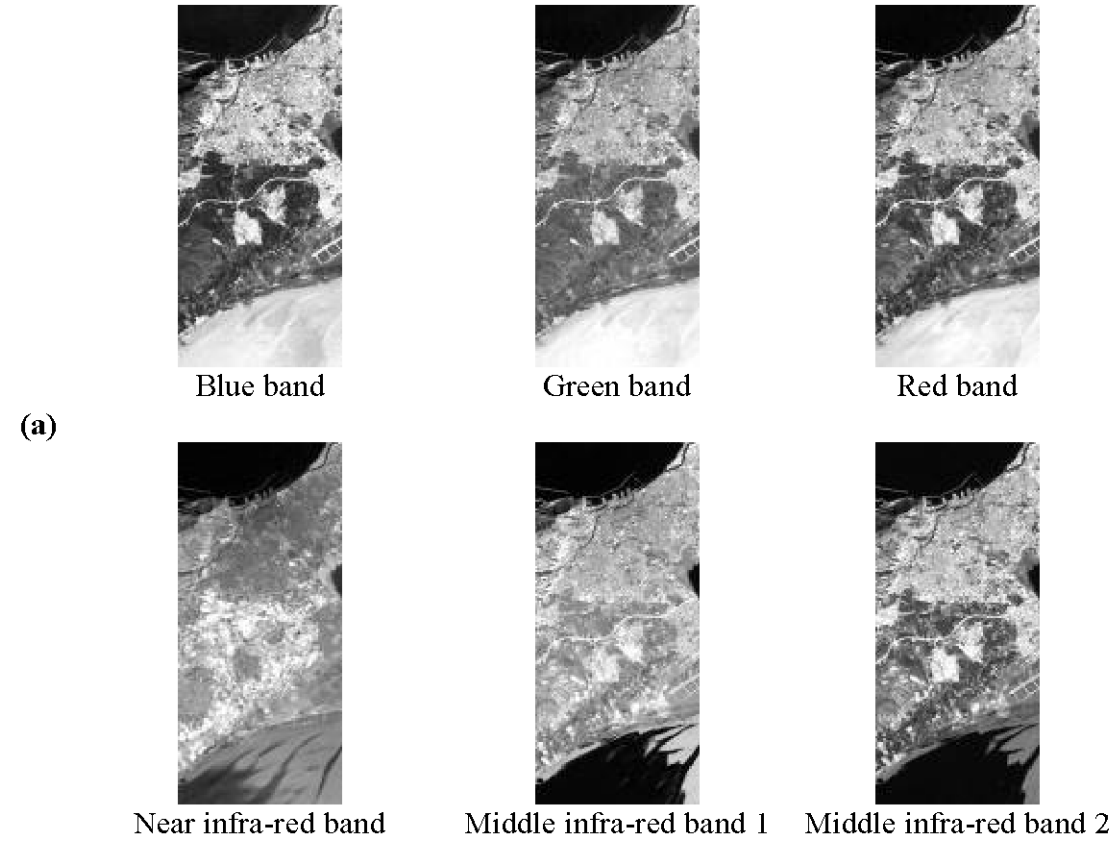

Figure 4. Real multispectral images. (a) Landsat ETM+ image (six bands) of Oran area (Algeria). (b) Formosat-2 image (four bands) of Toulouse area (France).

4.3. Results and discussion

The proposed methods are applied to synthetic and real datasets. In addition, the SMACC method [12] with the abundance fraction sum-to-one constraint is also applied to these datasets for comparison. This method, implemented in commercial software ENVI (ITT Corporation) [18], is one of the few approaches applicable to the underdetermined BSS model in multispectral remote sensing images, which is not, for example, the case of the method described in [25]. Let us stress here, that the SMACC method requires the number of endmembers (which corresponds to the number of clusters) to be known. This number is automatically detected by our methods and is provided to the SMACC method. SMACC uses a convex cone model to identify image endmember spectra. Extreme points (brightest pixels in image) are used to determine a convex cone, which defines the first endmember. A constrained oblique projection is then applied to the existing cone to derive the next endmember. The cone is increased to include the new endmember. The process is repeated until the specified number of endmembers is found.

Note here, that the optimal number of clusters automatically detected by our methods is 8 for the first synthetic dataset, and 10 for the second one, which is consistent with the number of created synthetic abundance maps in the two datasets. For the real multispectral images, the optimal number of clusters automatically detected by our methods is 18 for the Landsat ETM+ image, and 11 for the Formosat-2 image. For each real dataset, some extracted sources (abundance maps) correspond to the same thematic class of land. We therefore manually assigned these abundance maps to a unique class after the extraction stage. Thus, the final result is 11 abundance maps for Landsat ETM+ image, and 7 abundance maps for Formosat-2 image. These abundance maps are

assigned to thematic classes of land.

To verify (especially for the real multispectral images) the existence of single-source zones, we plot (Figs. 5 and 6) the histograms of the single-source zone detection parameter defined in (17) on the entire images, by exploring the spatial domain, using 5-by-5 pixel adjacent zones. These histograms show that this detection parameter is very close to 1 in some zones, which are single-source zones, while it is significantly lower than 1 in the other zones, which are multi-source zones.

(a)

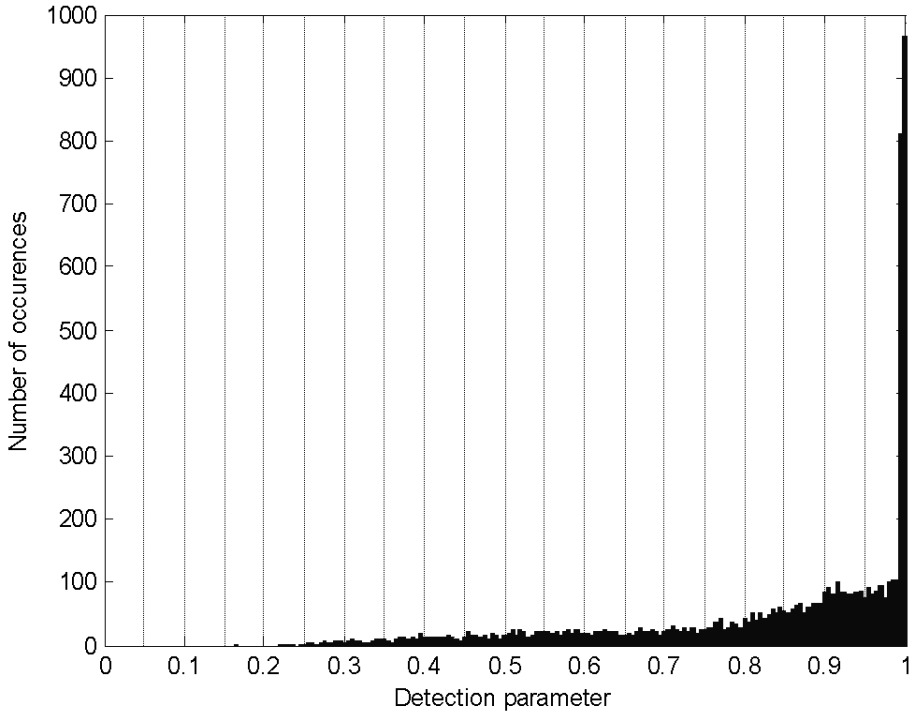

(b)

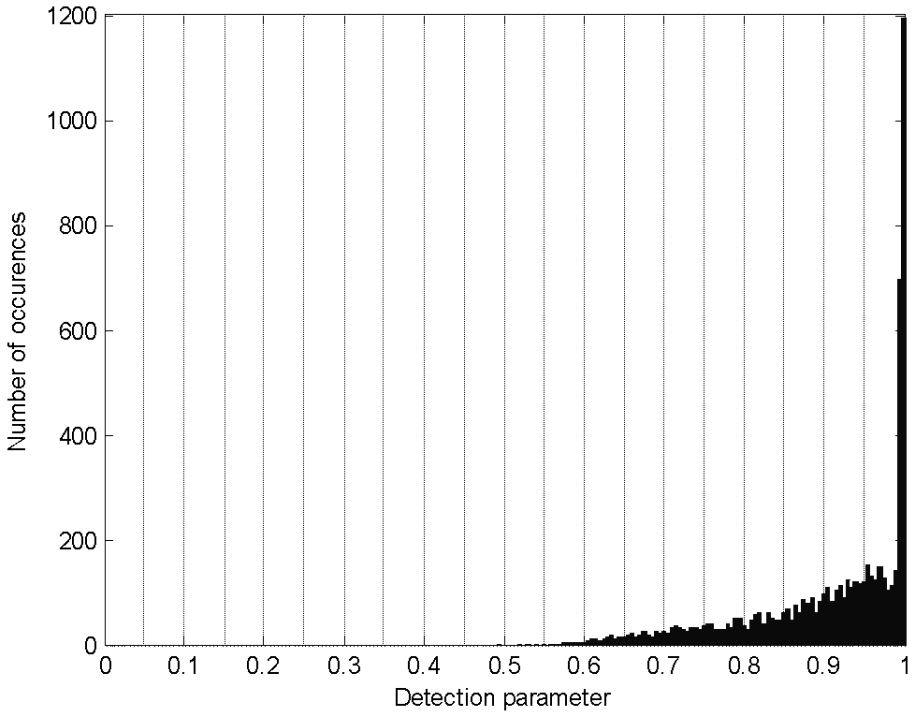

Figure 5. Histogram of the detection parameter for synthetic datasets. (a) First dataset. (b) Second dataset.

(a)

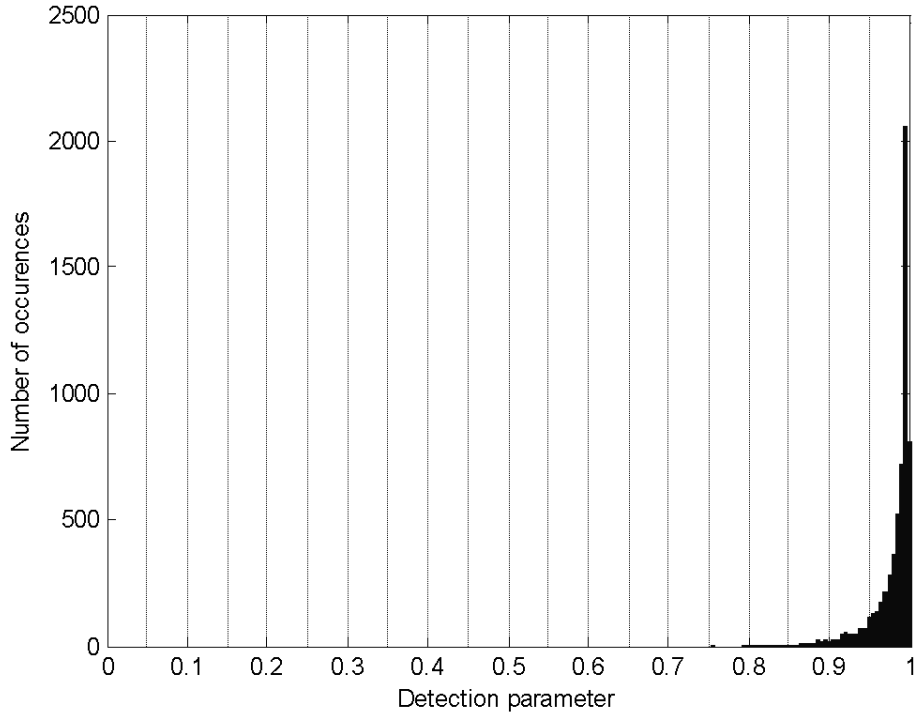

(b)

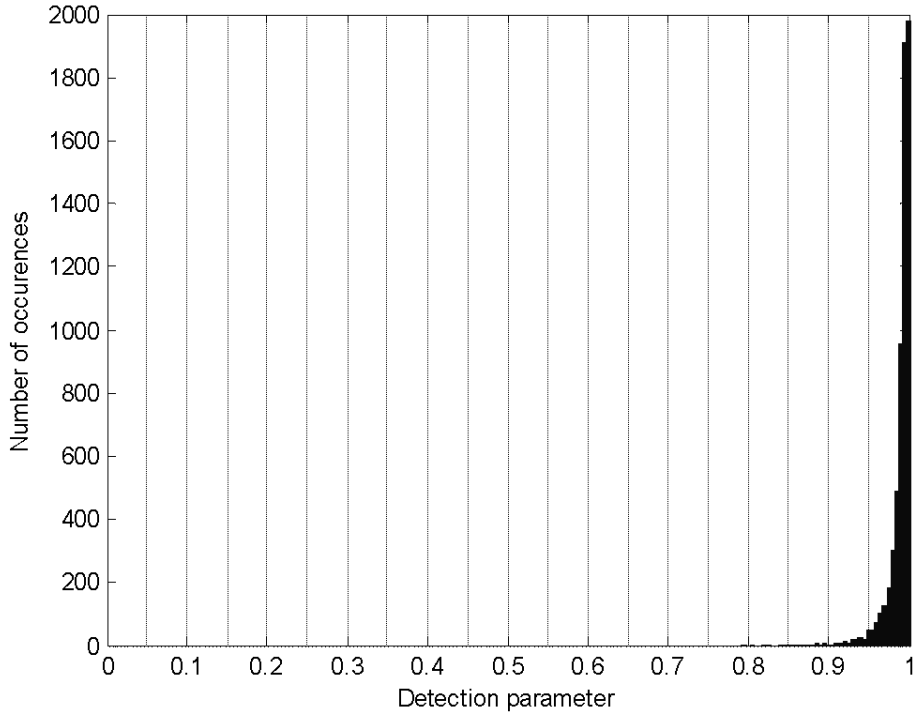

Figure 6. Histogram of the detection parameter for real datasets. (a) Landsat ETM+ image. (b) Formosat-2 image.

In order to further show that single-source and multiple-source analysis zones may be distinguished by the corresponding values of the detection parameter, we first select a single-source zone for each pure material, from the tested datasets. For each pure material, we also select a multiple-source zone, where this pure material is dominant. We compute the values of the detection parameter defined in (17) for all these zones. Results are shown in Figs. 7 and 8. From these results, we note that the detection parameter takes significantly lower values in multiple-source zones than in single-source zones. Therefore, it is a pertinent parameter for detecting single-source zones.

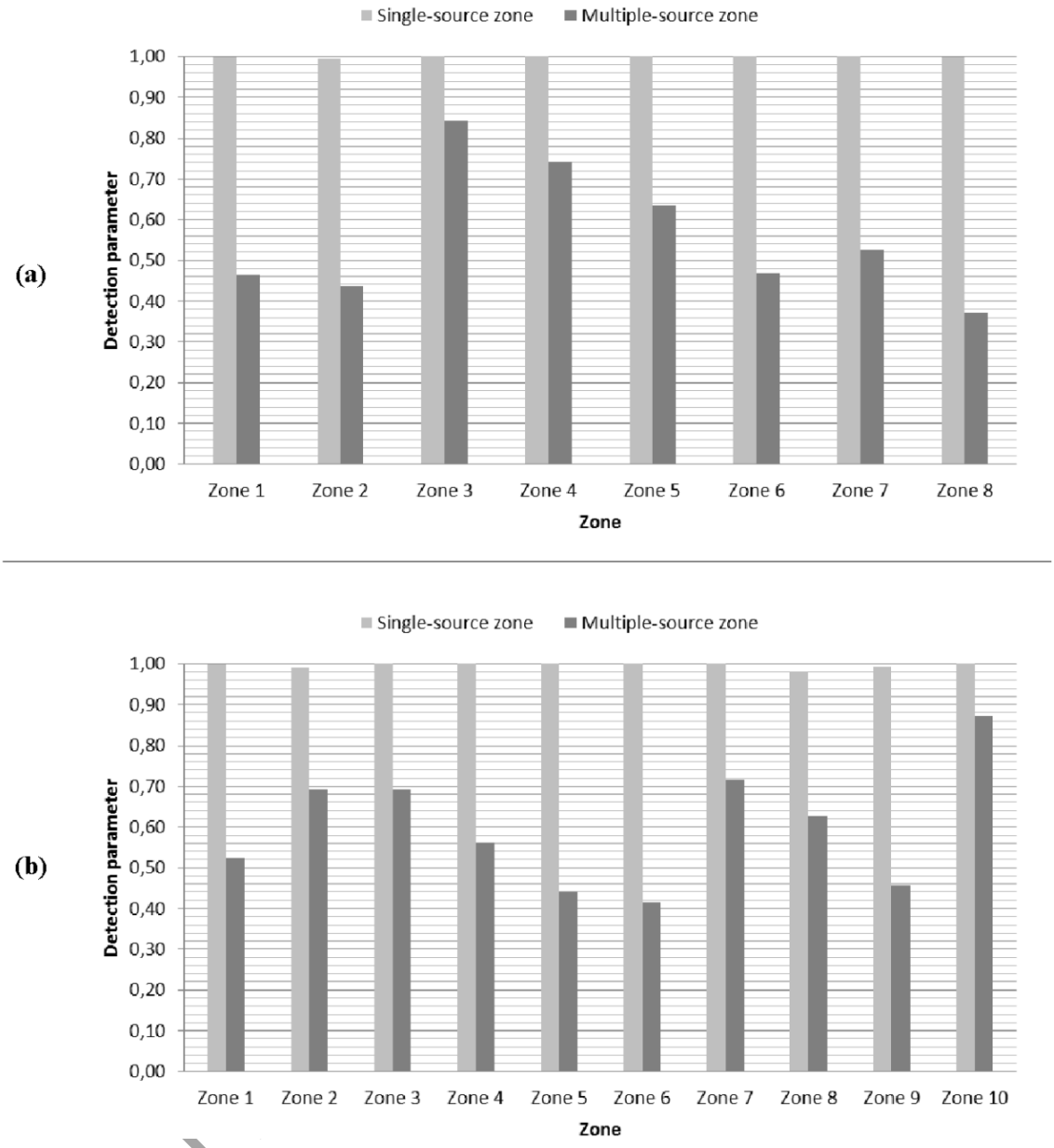

Figure 7. Detection parameter in single-source and multiple-source zones for synthetic datasets. (a) First dataset. (b) Second dataset.

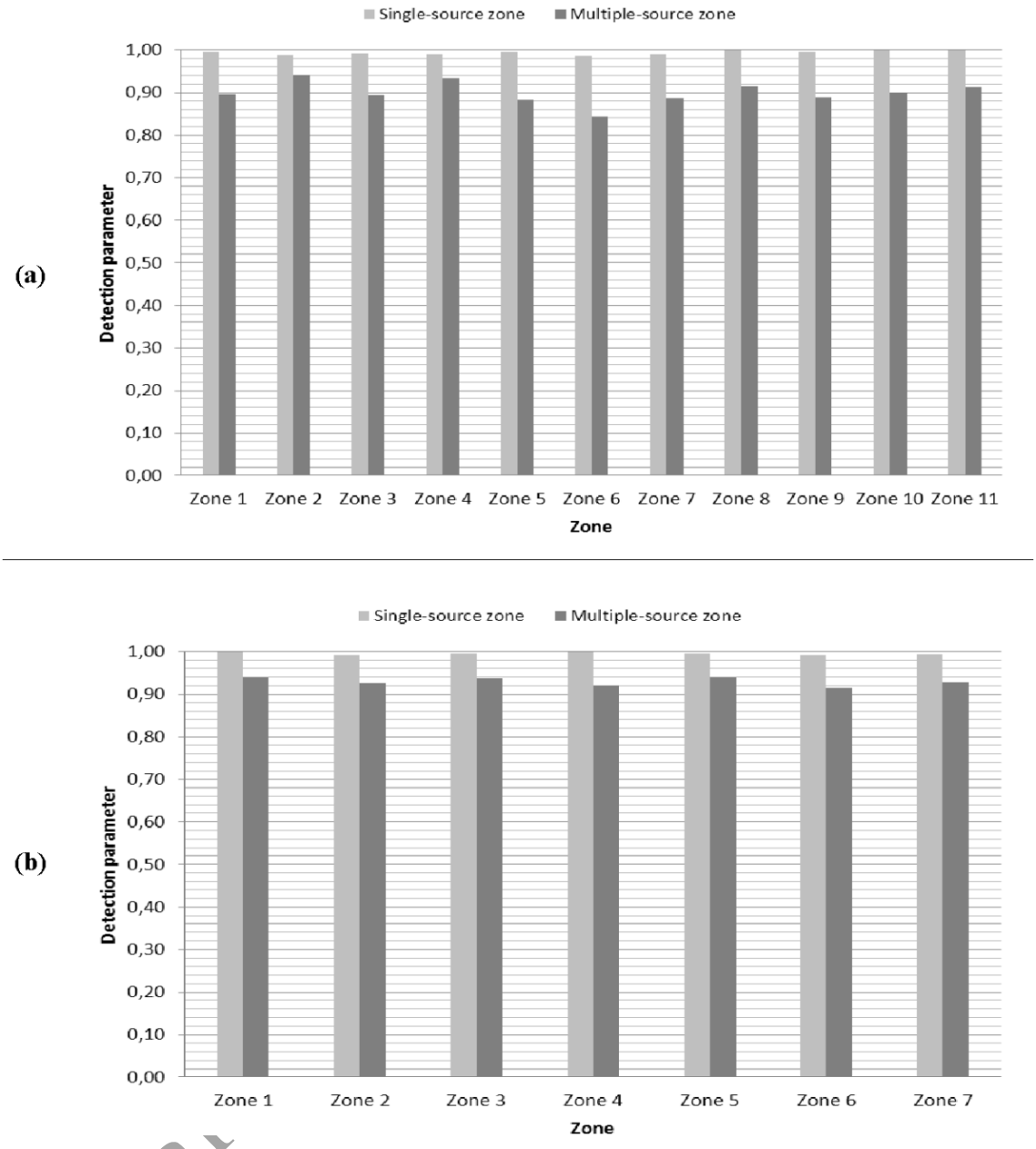

Figure 8. Detection parameter in single-source and multiple-source zones for real datasets. (a) Landsat ETM+ image. (b) Formosat-2 image.

The abundance maps (sources) estimated by the 2D-Corr-NLS method and SMACC are given in Figs. 9-12, for synthetic and real datasets. The NMSE criterion (%) is provided in Tables 1 and 2, respectively for the first and second synthetic datasets. The extraction accuracies (%) averaged over all abundance maps are given in Figs. 13 and 14.

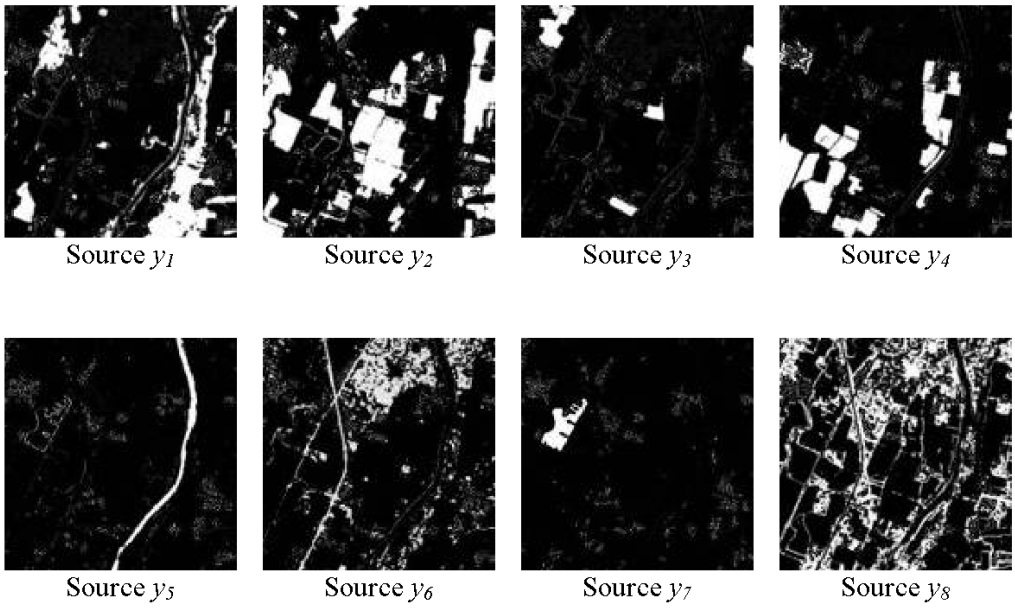

Figure 9. First synthetic sources (abundance maps) estimated by (a) 2D-Corr-NLS method, (b) SMACC method.

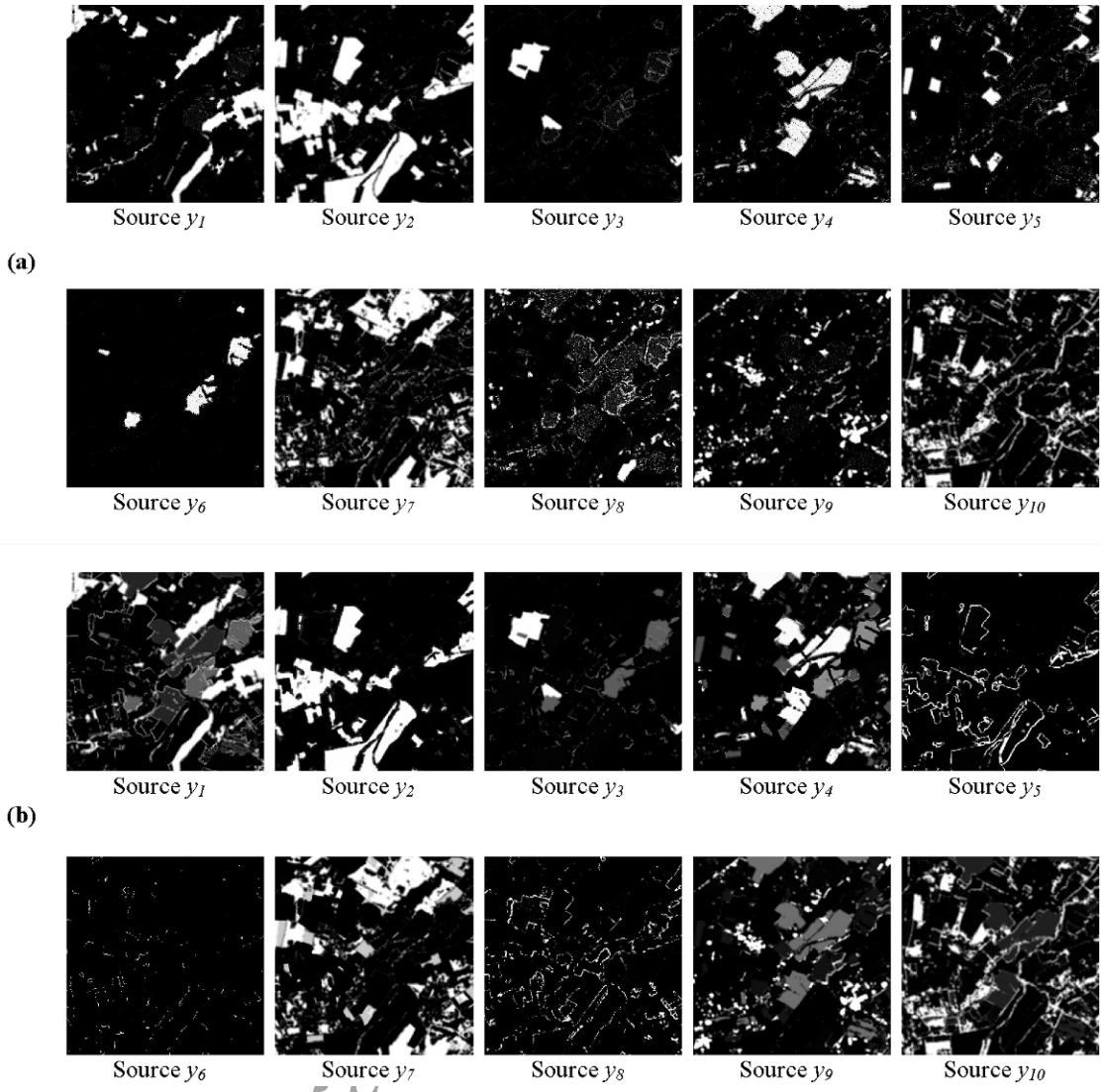

Figure 10. Second synthetic sources (abundance maps) estimated by (a) 2D-Corr-NLS method, (b) SMACC method.

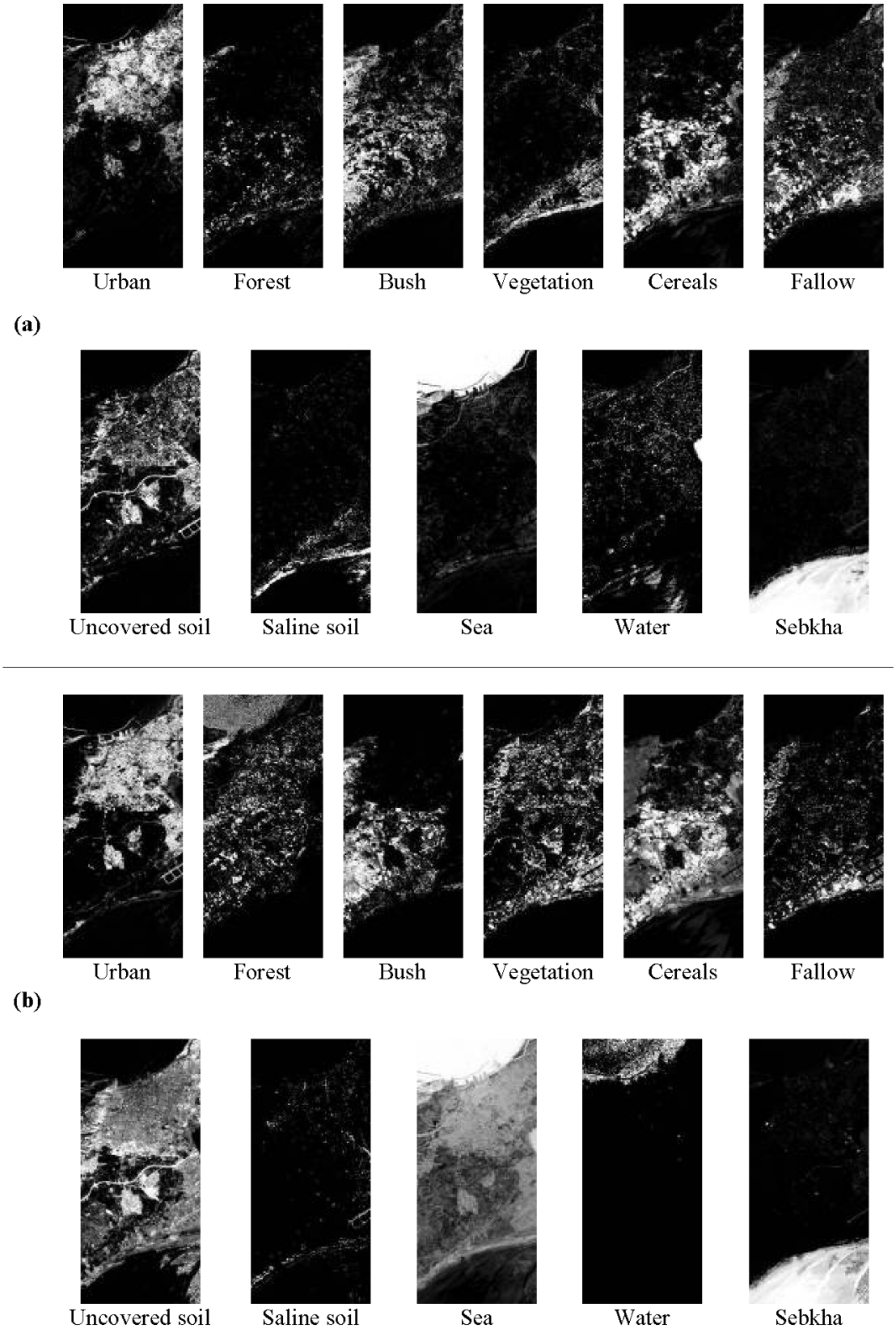

Figure 11. Real sources (abundance maps) estimated from the Landsat ETM+ image by (a) 2D-Corr-NLS method, (b) SMACC method.

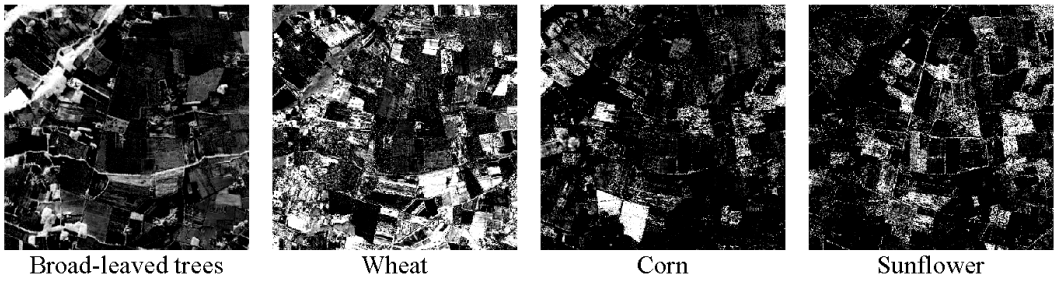

(a)

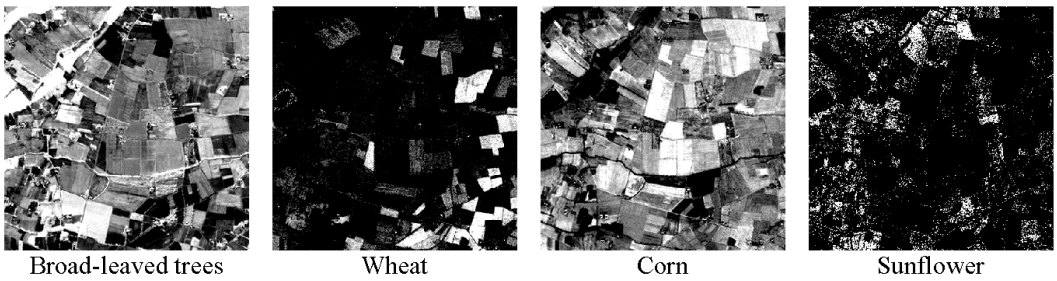

(b)

Figure 12. Real sources (abundance maps) estimated from the Formosat-2 image by (a) 2D-Corr-NLS method, (b) SMACC method.

Table 1. NMSE (%) for the first synthetic dataset. (a) All pixels. (b) Pure pixels. (c) Mixed pixels.

Method	Source s_1	Source s_2	Source s_3	Source s_4	Source s_5	Source s_6	Source s_7	Source s_8	Mean
(a)									
2D-Corr-NLS	0.99	0.00	0.40	0.57	7.44	1.90	1.25	0.15	1.59
SMACC	3.71	0.55	45.25	12.01	22.98	112.95	4.67	4.55	25.83
(b)									
2D-Corr-NLS	0.03	0.00	0.04	0.01	0.05	0.26	0.03	0.04	0.06
SMACC	1.74	0.04	17.57	5.08	5.98	112.89	0.40	3.90	18.45
(c)									
2D-Corr-NLS	3.54	0.01	2.39	3.18	25.87	2.90	8.89	0.24	5.88
SMACC	8.93	3.19	198.81	44.56	65.33	112.98	31.45	5.06	58.79

Table 2. NMSE (%) for the second synthetic dataset. (a) All pixels. (b) Pure pixels. (c) Mixed pixels.

Method	Source s_1	Source s_2	Source s_3	Source s_4	Source s_5	Source s_6	Source s_7	Source s_8	Source s_9	Source s_{10}	Mean
(a)											
2D-Corr-NLS	5.51	0.35	5.77	8.72	11.59	19.95	1.33	54.78	2.21	0.32	11.05
SMACC	21.26	6.66	21.25	41.01	132.47	102.20	18.48	133.47	27.74	2.18	50.67
(b)											
2D-Corr-NLS	0.17	0.00	0.41	2.75	0.09	3.01	0.02	23.98	2.63	0.08	3.31
SMACC	8.35	0.06	13.25	34.66	100.05	100.00	16.33	100.00	117.66	4.04	49.44
(c)											
2D-Corr-NLS	13.94	1.18	21.73	22.11	23.72	54.19	2.71	74.78	2.13	0.40	21.69
SMACC	41.65	22.32	45.12	55.28	166.65	106.66	20.75	155.20	11.56	1.57	62.68

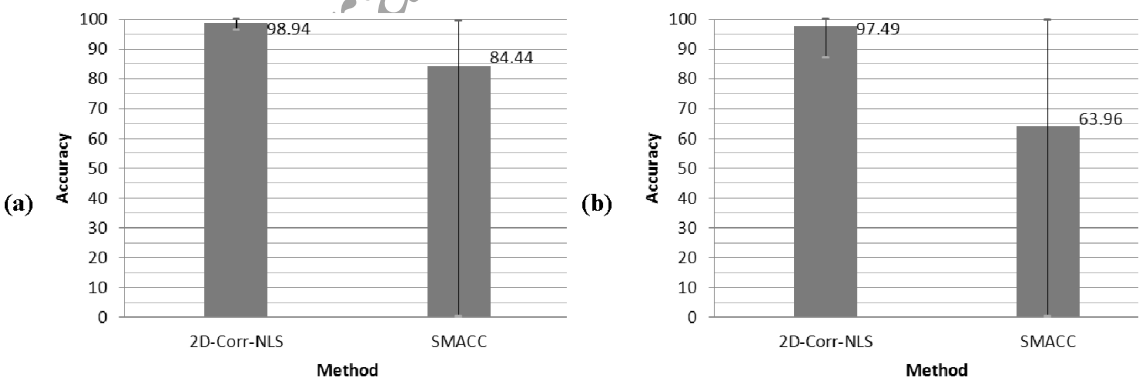

Figure 13. Overall extraction accuracies (%) for synthetic datasets. (a) First dataset. (b) Second dataset.

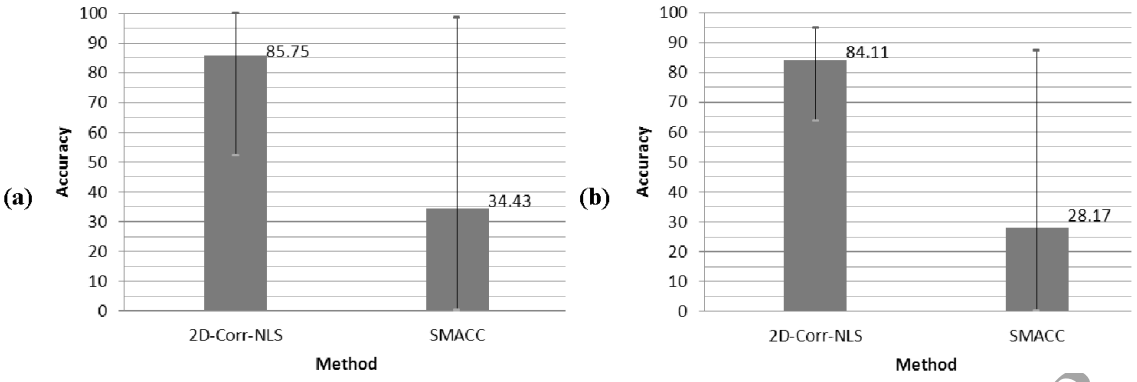

Figure 14. Overall extraction accuracies (%) for real datasets. (a) Landsat ETM+ image. (b) Formosat 2 image.

Globally, Table 1 and Figs. 9 and 10 show that the 2D-Corr-NLS method yields better performance than SMACC for synthetic datasets, especially, for extraction of source s_6 in the first synthetic dataset, and sources s_5, s_6, and s_8 in the second dataset. The mean improvement of the NMSE is about 24% for our 2D-Corr-NLS method as compared to SMACC for the first dataset, and about 39% for the second synthetic dataset. Fig. 13 shows that, in terms of overall extraction accuracies, the best results are also obtained with our 2D-Corr-NLS method for the two synthetic datasets.

For the real multispectral images, Figs. 11, 12 and 14 show that our 2D-Corr-NLS method yields better performance than SMACC: the improvement of the overall extraction accuracy is more than 51% for the Landsat ETM+ image, and about 56% for the Formosat-2 image. Figs. 11(b) and 12(b), which correspond to the abundance maps extracted by the SMACC method, show that the abundance maps of some classes are not clearly extracted. On the contrary, Figs. 11(a) and 12(a), which correspond to the abundance maps extracted by the 2D-Corr-NLS method, show a significant improvement for abundance maps extraction of the different classes of land cover.

5. Conclusion

In this paper, two unsupervised methods, called 2D-Corr-NLS and 2D-Corr-NMF, were proposed for spatial unmixing of multispectral images. These methods rely on a spatial correlation-based SCA approach, combined with clustering and approaches based on non-negativity constraints. In particular, the proposed methods are applicable to the globally underdetermined BSS model in multispectral remote sensing images.

Compared to the SMACC method, and according to the results obtained in these investigations (24% and 39% mean improvement of the normalized mean squared error for synthetic datasets, and more than 51% and 55% improvement of the overall extraction accuracy for real datasets), the proposed methods are very attractive for unmixing multispectral remote sensing images.

Future extensions of this work will be aimed at testing our methods for spatial unmixing of hyperspectral images. Another future extension may consist in testing other approaches for the detection stage of our methods, e.g. based on the variance of the ratio of observations.

Acknowledgments

We would like to thank D. Ducrot for providing us with the Formosat-2 image and classification result associated with a remote sensing image that we used to derive our synthetic datasets.

References

[1] F. Abrard, Y. Deville, A time-frequency blind signal separation method applicable to underdetermined mixtures of dependent sources, Signal Processing 85(7) (2005) 1389-1403.

[2] J.C. Bezdek, Pattern recognition with fuzzy objective function algorithms, Springer, 1981.

[3] J. M. Bioucas-Dias, A. Plaza, An overview on hyperspectral unmixing: geometrical, statistical, and sparse regression based approaches, in: Proceedings of the IEEE International Conference on Geoscience and Remote Sensing Symposium, 2011, pp. 1135-1138.

[4] A.O. Boudraa, Dynamic estimation of number of clusters in data sets, Electronics Letters 35(19) (1999) 1606-1607.

[5] A. Cichocki, R. Zdunek, S.I. Amari, New Algorithms for Non-Negative Matrix Factorization in Applications to Blind Source Separation, in: Proceedings of the IEEE International Conference on Acoustics, Speech and Signal Processing, 2006, pp. 621-624.

[6] A. Cichocki, R. Zdunek, A.H. Phan, S.I. Amari, Nonnegative Matrix and Tensor Factorizations: Applications to Exploratory Multi-way Data Analysis and Blind Source Separation, John Wiley & Sons, 2009.

[7] P. Comon, C. Jutten, Handbook of Blind Source Separation: Independent Component Analysis and Applications, Academic Press, Oxford, UK, 2010.

[8] Y. Deville, M. Puigt, Temporal and time-frequency correlation-based blind source separation methods. Part I: determined and underdetermined linear instantaneous mixtures, Signal Processing 87(3) (2007) 374-407.

[9] D. Donoho, V. Stodden, When does non-negative matrix factorization give a correct decomposition into parts? in: Proceedings NIPS 16, 2003, pp. 1141-1149.

[10] Y. Fukayama, M. Sugeno, A new method of choosing the number of clusters for fuzzy c-means method, in: Proceedings of the 5th Fuzzy Systems Symposium, 1989, pp. 247-250.

[11] G. Gan, C. Ma, J. Wu, Data Clustering: Theory, Algorithms, and Applications, SIAM, 2007.

[12] J. Gruninger, A.J. Ratkowski, M.L. Hoke, The sequential maximum angle convex cone (SMACC) endmember model, in: Proceedings of the SPIE Algorithms and Technologies for Multispectral, Hyperspectral, and Ultraspectral Imagery X, vol. 5425, 2004, pp. 1-14.

[13] J.H. Han, D.S. Huang, Z.L. Sun, Y.M. Cheung, A Novel Mixed Pixels Unmixing Method for Multispectral Images, in: Proceedings of the IEEE International Joint Conference on Neural Networks, vol. 4, 2004, pp. 2541-2545.

[14] D.C. Heinz, C.I. Chang, Fully Constrained Least Squares Linear Spectral Mixture Analysis Method for Material Quantification in Hyperspectral Imagery, IEEE Transactions on Geoscience and Remote Sensing 39(3) (2001) 529-545.

[15] J. Herault, C. Jutten, B. Ans, Détection de grandeurs primitives dans un message composite pour une architecture de calcul neuromimétique en apprentissage non supervisé, in: GRETSI, 1985, pp. 1017-1022.

[16] J. Herault, C. Jutten, Space or time adaptive signal processing by neural network models, in: International Conference on Neural Networks for Computing, 1986.

[17] A. Ifarraguerri, C. Chang, Multispectral and Hyperspectral Image Analysis with Convex Cones, IEEE Transactions on Geoscience and Remote Sensing 37(2) (1999) 756-770.

[18] ITT Corporation: ENVI – Solutions for Data Vis. and Image Analysis. http://www.ittvis.com/envi/.

[19] A. Jourjine, S. Rickard, Ö. Yilmaz, Blind separation of disjoint orthogonal signals: Demixing N sources from 2 mixtures, in: Proceedings of the IEEE International Conference on Acoustic, Speech, and Signal Processing, 2000, pp. 2985-2988.

[20] C. Jutten, J. Herault, Blind separation of sources. Part i: an adaptive algorithm based on neuromimetic architecture, Signal Processing 24(1) (1991) 1-10.

[21] M.S. Karoui, Y. Deville, S. Hosseini, A. Ouamri, D. Ducrot, Contribution of non-negative matrix factorization to the classification of remote sensing images, in: Proceedings of the SPIE Europe Remote Sensing Conference : Image and Signal Processing for Remote Sensing XIV, SPIE vol. 7109, 2008.

[22] M.S. Karoui, Y. Deville, S. Hosseini, A. Ouamri, D. Ducrot, Improvement of remote sensing multispectral image classification by using independent component analysis, in: Proceedings of the First IEEE Workshop on Hyperspectral Image and Signal Processing, 2009.

[23] N. Keshava, J.F. Mustard, Spectral Unmixing, IEEE Signal Processing Magazine, vol. 19 (2002) 44-57.

[24] D.J. Kim, Y.W. Park, D.J. Park, A Novel Validity Index for Determination of the Optimal Number of Clusters, IEICE Transactions on Information and Systems E84-D(2) (2001) 281-285.

[25] I. Kopriva, A. Cichocki, Blind multispectral image decomposition by 3D nonnegative tensor factorization, Optics Letters 34(14) (2009) 2210-2212.

[26] S.H. Kwon, Cluster validity index for fuzzy clustering, Electronics Letters 34(22) (1999) 2176-2177.

[27] C.L Lawson, R.J. Hanson, Solving Least Squares Problems, SIAM, 1974.

[28] D.D. Lee, H.S. Seung, Learning the parts of objects by non-negative matrix factorization, Nature 401 (1999) 788-791.

[29] D.D. Lee, H.S. Seung, Algorithms for non-negative matrix factorization, Advances in Neural Information Processing Systems 13, MIT Press (2001) 556-562.

[30] I. Meganem, Y. Deville, M. Puigt, Blind separation methods based on correlation for sparse possibly-correlated images, in: Proceedings of the IEEE International Conference on Acoustics, Speech, and Signal Processing, 2010, pp. 1334-1337.

[31] Y. Moudden, J. Bobin, Hyperspectral BSS Using GMCA With Spatio-Spectral Sparsity Constraints, IEEE Transactions on Image Processing 20(3) (2011) 872-879.

[32] J.M.P. Nascimento, J.M. Bioucas-Dias, Does Independent Component Analysis Play a Role in Unmixing Hyperspectral Data? IEEE Transactions on Geoscience and Remote Sensing 43(1) (2005) 175-187.

[33] A. Pacheco, H. McNairn, Evaluating multispectral remote sensing and spectral unmixing analysis for crop residue mapping, Remote Sensing of Environment 114 (2010) 2219-2228.

[34] N.R. Pal, J.C. Bezdek, On cluster validity for the fuzzy c-means model, IEEE Transactions on Fuzzy Systems 3(3) (1995) 370-379.

[35] M. Parente, A. Plaza, Survey of geometric and statistical unmixing algorithms for hyperspectral images, in: Proceedings of the Second IEEE Workshop on Hyperspectral Image and Signal Processing, 2010.

[36] A. Quirin, J. Korczak, Representation of Genetic Individuals for Unmixing Multispectral Data, in: Proceedings of the IEEE Congress on Evolutionary Computation, 2005, pp. 1325-1331.

[37] H. Ren, Y.L. Chang, Multispectral subpixel detection using least square unmixing, in: Proceedings of the IEEE International Conference on Geoscience and Remote Sensing Symposium, 2006, pp. 2754-2756.

[38] J. Settle, On Constrained Energy Minimization and the Partial Unmixing of Multispectral Image, IEEE Transactions on Geoscience and Remote Sensing 40(3) (2002) 718-721.

[39] N. L. Xie, G.A. Beni, A validity measure for fuzzy clustering, IEEE Transactions on Pattern Analysis and Machine Intelligence 13(8) (1991) 841-847.